The Astrophysical Journal, 691:L151–L155, 2009 February 1 doi:10.1088/0004-637X/691/2/L151

RELATIONSHIP BETWEEN A CORONAL MASS EJECTION-DRIVEN SHOCK AND A CORONAL METRIC TYPE II BURST

Y. Liu, J. G. Luhmann, S. D. Bale, and R. P. Lin
Space Sciences Laboratory, University of California, Berkeley, CA 94720, USA; liuxying@ssl.berkeley.edu.
Received 2008 November 16; accepted 2008 December 16; published 2009 January 19

ABSTRACT

It has been an intense matter of debate whether coronal metric type II bursts are generated by coronal mass ejection (CME)-driven shocks or flare blast waves. Using unprecedented high-cadence observations from *STEREO*/SECCHI, we investigate the relationship between a metric type II event and a shock driven by the 2007 December 31 CME. The existence of the CME-driven shock is indicated by the remote deflection of coronal structures, which is in good timing with the metric type II burst. The CME speed is about 600 km s^{-1} when the metric type II burst occurs, much larger than the Alfvén speed of 419–489 km s^{-1} determined from band splitting of the type II burst. A causal relationship is well established between the metric and decametric–hectometric type II bursts. The shock height–time curve determined from the type II bands is also consistent with the shock propagation obtained from the streamer deflection. These results provide unambiguous evidence that the metric type II burst is caused by the CME-driven shock.

Key words: shock waves – Sun: coronal mass ejections (CMEs) – Sun: flares – Sun: radio radiation

Online-only material: mpeg animation

1. INTRODUCTION

Type II bursts are narrowband radio emissions typically drifting downward in frequency (e.g., Payne-Scott et al. 1947; Wild et al. 1953). They have been known as remote signatures of a shock moving through the solar corona and heliosphere (Nelson & Melrose 1985). The origin of the shock in the corona that manifests as type II bursts at meter wavelengths is a long-standing source of controversy in solar and space physics. The shock is either attributed to a sudden short-range expansion due to flare impulsive heating (flare blast waves) or piston driven by coronal mass ejections (CMEs; e.g., Gopalswamy et al. 1998; Cliver et al. 1999, 2005; Pick et al. 2006; Vršnak & Cliver 2008). Flare ejecta are also considered as a possible material driver for the shock (e.g., Gopalswamy et al. 1998; Klein et al. 1999); the distinction between flare ejecta and CMEs, however, is probably not fundamental, especially in terms of the ejection mechanisms (Cliver 1999, and references therein). There is a close timing between the CME acceleration and flare impulsive phase when a metric type II burst occurs (e.g., Zhang et al. 2001; Cliver et al. 2005), which makes it very difficult to distinguish the two sources. This is the primary reason for a rather chaotic state of the art even 60 years after the discovery of coronal type II bursts.

If the shocks that generate metric type II bursts are freely propagating blast waves originating from solar flares, they would decay quickly and thus cannot reach interplanetary space. CME-driven shocks, however, have energy continuously supplied by the driver and would be more energetic and long-lived. This difference is of particular relevance to space weather forecasting and studies of solar energetic particles (SEPs). SEP events have been classified into gradual events accelerated by CME-driven shocks and impulsive events produced by reconnection processes in solar flares (Cane et al. 1986; Reames 1999); more recent observations suggest the existence of hybrid cases (e.g., Cohen et al. 1999; Mason et al. 1999), calling this picture into question. If a CME-driven shock can form low in the corona, the shock may contribute to the initial acceleration of SEPs which is generally thought to be of flare origin; impulsive SEP material from the associated flare may also be swept and further accelerated by the CME-driven shock, leading to hybrid SEPs. Drift rates of type II bursts are often used to predict the arrival time of interplanetary shocks at the Earth (e.g., Liu et al. 2008). If the source of metric type II bursts is a CME-driven shock, the prediction of the shock arrival time can be made at the early stage of shock propagation, thus increasing the warning time. Therefore, the origin of coronal shocks is not only an outstanding theoretical concern but also has important consequences for studies of space weather and SEPs.

An unambiguous clarification of the shock origin relies on high-cadence imaging observations of the low corona where early CME acceleration occurs. The early CME evolution could be easily missed by a low-cadence coronal patrol. For example, the Extreme-Ultraviolet Imaging Telescope (EIT) aboard the *Solar and Heliospheric Observatory* (*SOHO*) has a cadence rate of 12 minutes at 195 Å and a field of view (FOV) of 1.5 $R_\odot$ (where $R_\odot$ is the solar radius); a CME with a speed of 500 km s^{-1} as commonly observed will move out of the EIT FOV within 12 minutes. High-cadence observations of early CME kinematics, which allow a comparison with a certain range of Alfvén speeds, can determine the distance and time of shock formation. This is key to providing a definite answer as to whether a coronal shock is driven by a CME, but which so far has been lacking. In this Letter, we report high-cadence imaging observations of a limb CME on 2007 December 31 made with the Sun–Earth Connection Coronal and Heliospheric Investigation (SECCHI) aboard the *Solar Terrestrial Relations Observatory* (*STEREO*; Howard et al. 2008) and its relationship to a metric type II burst. The Extreme-Ultraviolet Imagers (EUVI) of SECCHI have a cadence of 2.5 minutes at 171 Å and cover an FOV out to 1.7 $R_\odot$, and the SECCHI inner coronagraph COR1 has a cadence of 5 minutes and an FOV of 1.4–4 $R_\odot$. The high observational capabilities of *STEREO*/SECCHI provide an unprecedented opportunity to investigate the coronal dynamics associated with CMEs.

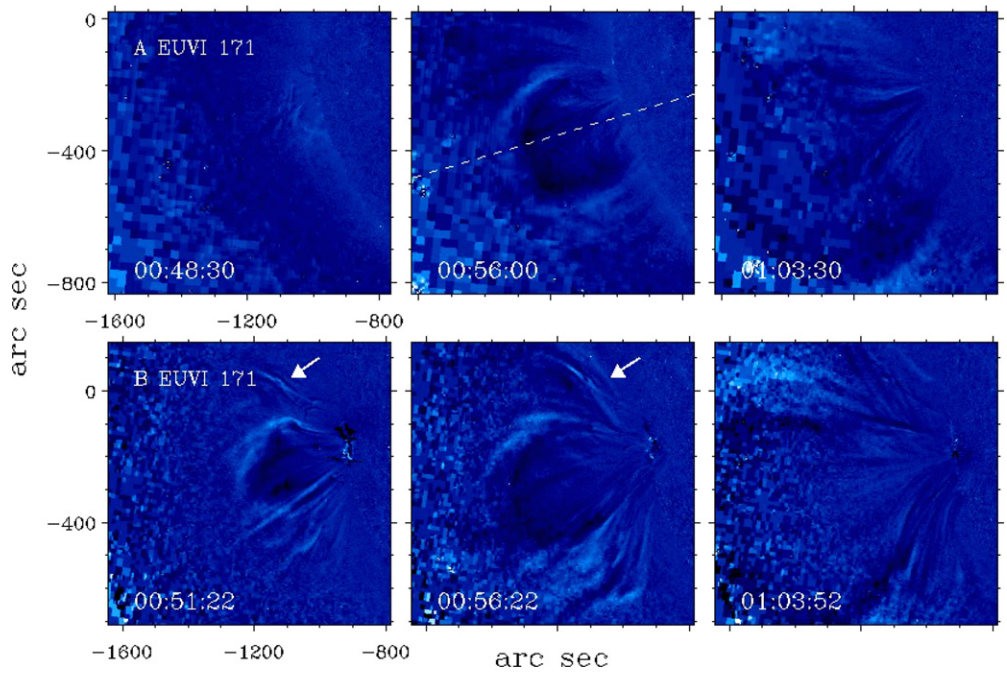

Figure 1. Running difference images of EUVI aboard *STEREO A* (top) and *B* (bottom) at 171 Å showing the early CME evolution. The arrow indicates the deflection of coronal structures by the CME-driven shock. The dashed line marks the direction from the center of the Sun (origin of the coordinates) along which the height of the CME front is measured. The solar ecliptic north is up.

2. OBSERVATIONS AND RESULTS

We chose a limb event because the CME height in the low corona can be directly measured without using extrapolation; projection effects in the height and speed measurements can also be minimized. This CME is typical in many of its characteristics such as fast expansion and close timing with the flare impulsive phase and the metric type II onset (e.g., Zhang et al. 2001; Cliver et al. 2005). The results obtained here would be widely representative of fast CMEs.

Figure 1 shows running difference images of EUVI at the nascent stage of the 2007 December 31 CME. The *STEREO* twin spacecraft, one preceding the Earth (*STEREO A*) and the other trailing behind (*STEREO B*) in the ecliptic plane, is separated by 43.°7 in longitude at this time. The CME occurs at the east limb in both *STEREO A* and *B* observations. It is first visible around 00:48:30 UT for *STEREO A* with an initial height of 1.09 $R_\odot$ from the center of the Sun; at about the same time (00:48:52 UT) *STEREO B* sees the CME front at about 1.21 $R_\odot$. There is a slight projection effect, but in general the measured height and speed are close to the true values. The CME quickly expands into a loop structure with two ends connected to the Sun.

Of particular interest is the deflection of coronal structures north of the CME. The coronal structures are pushed aside before the CME impinges on them, indicative of a pressure wave running ahead of the CME. The deflection first occurs at 00:51:22 UT as observed by *STEREO B* (see Figure 1), about 2.6 minutes before the onset of the metric type II burst; at this time, the CME front reaches a heliocentric distance of 1.36 $R_\odot$ along the direction shown in Figure 1. At the time of the metric type II onset, the CME has a velocity much larger than the Alfvén speed in the ambient corona (see below), so the pressure wave must have steepened into a shock. Deflections of remote coronal structures provide the best imaging evidence for CME-driven shocks (Gosling et al. 1974; Sheeley et al. 2000; Vourlidas et al. 2003). Flare loops rise after the CME has lifted off as seen by *STEREO B*, but they occur within a restricted area and apparently bear no relationship to the coronal structure deflection.

Composite images of SECCHI from *STEREO A* are shown in Figure 2 in order to give a panoramic view of the CME evolution from the low corona to large distances. The SECCHI imaging system also includes an outer coronagraph COR2 with an FOV 2.5–15 $R_\odot$ and cadence about 15 minutes, and an inner heliospheric imager (HI1) with an FOV 15–84 $R_\odot$ (20° across) and cadence 40 minutes. The quality of these images is compromised by the need for a composite display of limited size. A smooth transition of the CME is observed from EUVI to COR1, from COR1 to COR2, and finally from COR2 to HI1. The CME appears as a semicircular bright rim in EUVI but rises as a typical three-part structure in COR1. It is distorted into a concave-outward structure by a preexisting high-density heliospheric plasma sheet, as can be seen in COR2 and HI1. A large lateral expansion is also evident. The angular width of the CME subtended at the Sun center is about 21° at 00:56 UT (EUVI) and increases to 79° at 01:53:20 UT (COR2).

The shock also emerges from the low corona. It produces a kink in the streamer north of the CME (in COR1 at 01:15:18 UT), which quickly develops into a break point propagating along the streamer (in COR2 and HI1). The bend in the streamer keeps pace with the CME, but there is no direct contact between the streamer and the outermost edge of the CME. Although the shock cannot be directly imaged, its presence is revealed by its effect on nearby structures. A similar scenario is observed by the Large Angle Spectroscopic Coronagraph (LASCO) aboard *SOHO*, so there must be a shock running in front of the CME; a diffuse weak edge is discernible ahead of the CME front in LASCO difference images, indicative of a shock front. The shock is clearly driven by the CME, since the source region expansion caused by the flare energy release cannot persist to such large time (greater than 13 hr) and spatial (greater than 40 $R_\odot$) scales.

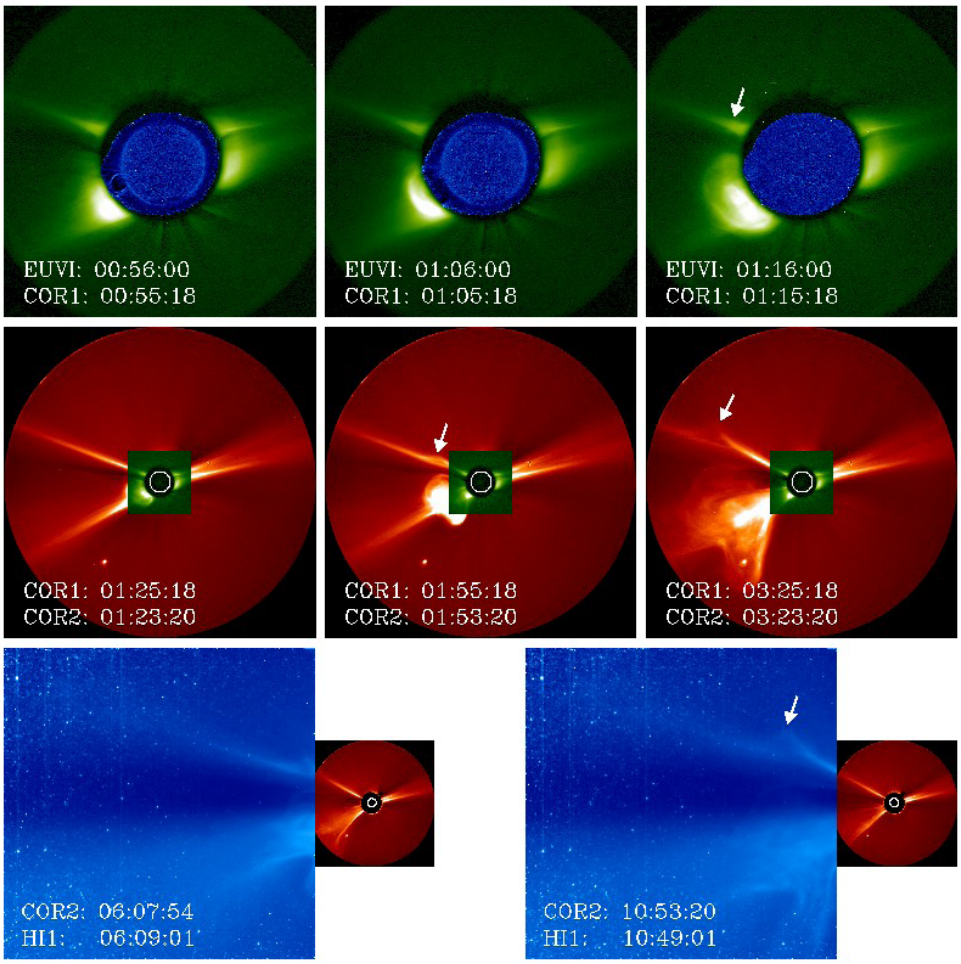

Figure 2. Composite images of EUVI at 171 Å and COR1 (top), COR1 and COR2 (middle), and COR2 and HI1 (bottom) on board *STEREO A*. Running difference images are used for EUVI to show a clear transition of the CME from EUVI to COR1. The arrow indicates the deflection of a streamer north of the CME by the CME-driven shock. The white circle represents the size and position of the solar disk. The solar ecliptic north is about 5°.4 from up to the left.

(An mpeg animation of this figure is available in the online journal.)

Height measurements are displayed in Figure 3 for the CME front along the direction shown in Figure 1 and the shock along the streamer north of the CME. The uncertainty in the measurements is estimated to be about 10 pixels in each image, which is roughly 0.02, 0.08, 0.15, and 0.72 $R_\odot$ for EUVI, COR1, COR2, and HI1 separately. The height of the shock is obtained by following the break point in the streamer visible in COR2 and HI1 observations of *STEREO A*; a distinct break point is not formed in EUVI and COR1 images, so the earlier shock propagation cannot be determined precisely. A polynomial fitting of the measurements is made feasible by the high-cadence observations. The early evolution of the CME observed by EUVI and COR1 has an acceleration about 158 and 166 m s^{-2} derived from a second-order polynomial fit of *STEREO A* and *B* observations, respectively; similar values of the CME speed are also observed by *STEREO A* and *B*. The CME speed at 1.5 $R_\odot$ (corresponding to the time 00:54 UT when a metric type II burst occurs) is ~600 km s^{-1}, much larger than the Alfvén speed at the same distance (see below). The CME is decelerating at later times, which is confirmed by the shock propagation. In the FOV of COR2 and HI1, the shock has a speed about of 740 km s^{-1} at 5 $R_\odot$ and an acceleration of −8.9 m s^{-2}. This speed as well as the CME angular width is consistent with the estimates of S. Yashiro (2008, private communication) from LASCO images.

Figure 4 shows the radio dynamic spectrum as well as the soft X-ray flux associated with the CME. The CME is accompanied by a C8.3 flare whose impulsive phase has a good timing with the early CME acceleration. A continuous frequency coverage from 180 MHz down to 2.5 kHz is obtained by combining observations from WAVES on board *STEREO* (SWAVES, 2.5 kHz to 16 MHz; Bougeret et al. 2008), the Bruny Island Radio Spectrometer (BIRS, 6–62 MHz; Erickson 1997) and the Learmonth spectrograph (25–180 MHz; data are available at http://www.ips.gov.au/Solar). The BIRS data within 16–25 MHz are plotted between the Learmonth and SWAVES measurements. The metric type II burst appears as multiple slowly drifting bands with a starting frequency of about 100 MHz. It begins around 00:54 UT, only within a few minutes of the flare impulsive phase. This close timing has been used as a strong argument for the flare origin of coronal shocks (e.g., Kundu 1965; Vršnak et al. 1995). Without high-cadence imaging observations of the low corona, flares as a candidate source for metric type II bursts cannot be completely ruled out. Two drifting bands, with a frequency ratio of 1.26, occurs between 50 and 100 MHz around 00:54 UT; they show a marked similarity in frequency drift rate and morphology. The radio instruments generally observe similar features in their frequency overlapping range. The BIRS data, however, show two parallel weak bands between 25 and 55 MHz around 00:54 UT that are

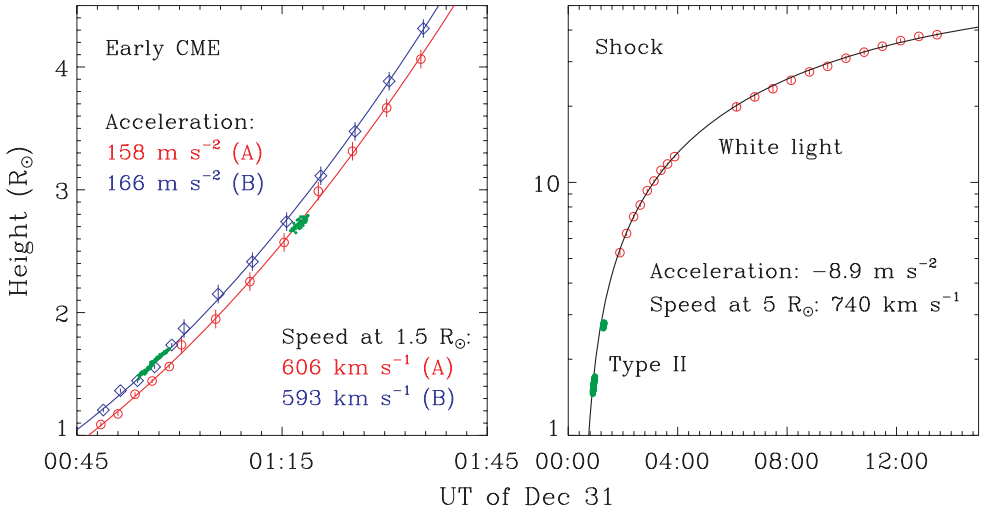

Figure 3. Height of the CME front (left) and shock (right) relative to the center of the Sun measured by *STEREO A* (red) and *B* (blue). Error bars indicate the uncertainty in the measurements. The solid lines represent the second-order polynomial fit of the imaging observations; the acceleration and speed (at certain distances) derived from the fit are also given. The green dots indicate the height determined from the lower branch of the harmonic type II bands.

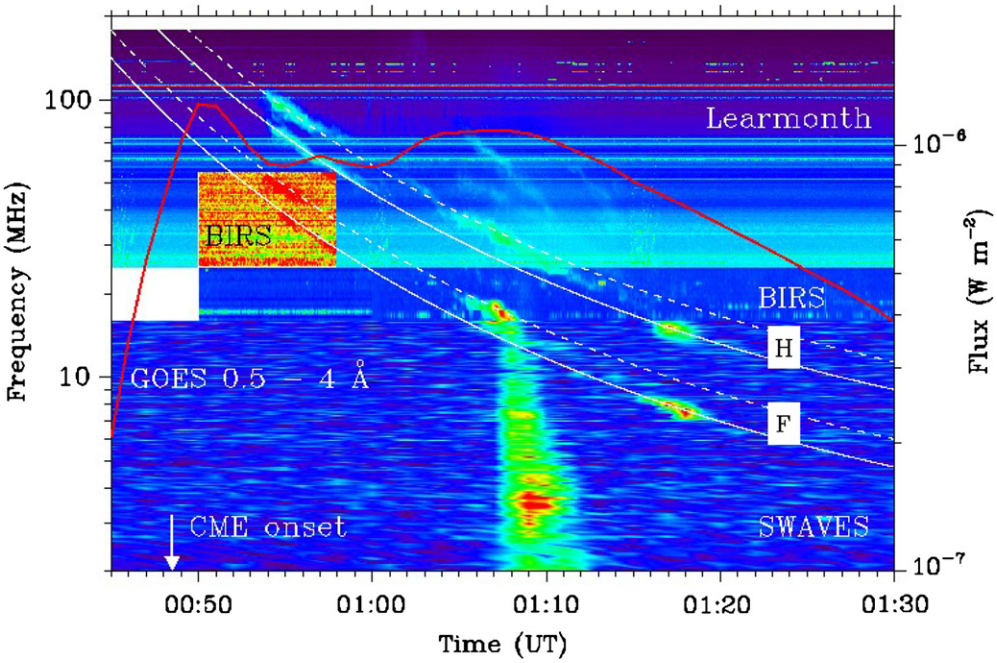

Figure 4. Dynamic spectrum (color shading) from the Learmonth spectrograph (top), BIRS (middle), and SWAVES aboard *STEREO A* (bottom). The *GOES* X-ray flux is denoted by the red line. The white lines represent the best fit of the frequency drift of the fundamental (F) and harmonic (H) type II bands upstream (solid) and downstream (dashed) of the shock. The vertical arrow indicates the time of the CME onset as observed by EUVI of *STEREO A*. An intense type III burst emanates from the type II band at 17 MHz around 01:07 UT and extends to 100 kHz. Unlike conventional type III bursts, it lags about 16 minutes behind the flare impulsive phase and does not have a counterpart at meter wavelengths, suggestive of a shock-associated event (Cane et al. 1981; Bougeret et al. 1998).

missed by the Learmonth measurements. Therefore, we use a patch from the BIRS data between 00:50 and 00:58 UT for this frequency range; a different color contrast has been applied to make the two bands discernible. These two bands have the same frequency ratio of 1.26, and each occurs at half frequencies of its high-frequency counterpart, suggestive of splitting at the fundamental and harmonic bands of the type II burst. The type II burst seems to extend to the decametric–hectometric (DH) domain (20–1 MHz); the SWAVES data show emissions around 01:16 UT at the fundamental and harmonic plasma frequencies without band splitting.

Band splitting of type II bursts has been shown to be a consequence of plasma radiation from the regions upstream and downstream of shocks (e.g., Smerd et al. 1975; Vršnak et al. 2001). The density jump ratio r_s across a shock can thus be estimated from the frequency ratio of the splitting bands given $f = 8.97\sqrt{n}$, where f (in units of kHz) is the plasma frequency and n (in units of cm^{-3}) is the plasma density. We obtain $r_s = 1.59$ for the current case. The shock Alfvén Mach number M_A (v/v_A, where v is the speed of the shock and v_A is the Alfvén speed) is related to r_s as

$$M_A = \sqrt{r_s}$$

for a parallel shock and

$$M_A = \sqrt{\frac{r_s(r_s+5)}{2(4-r_s)}}$$

for a perpendicular shock (Priest 1982; Vršnak et al. 2002). A small plasma beta has been assumed for the corona where metric type II bursts occur, which is usually true. The present density jump ratio results in $M_A = 1.26$–1.47 depending on the shock geometry. The shock Mach number in combination with the shock speed inferred from the frequency drift rate will provide an estimate of the Alfvén speed.

We use a coronal density model suitable for solar minimum (Saito et al. 1977) to convert frequencies of the type II bands into heliocentric distances. Uncertainty in the density model can be minimized by requiring consistency between the observed CME height and the calculated height of the type II emissions at the early stage of the CME evolution. The trace of the harmonic band corresponding to the upstream emissions of the shock is singled out and shown in Figure 3 as distances; a good agreement with the CME height is achieved by multiplying the density model by a factor of 1.3. The speed of the shock, obtained from a linear fit of the distances of the type II burst, is about 616 ± 1.9 km s^{-1}. (Note that radio imaging observations are not available for this event, so the exact location of the type II burst relative to the CME cannot be determined. Type II emissions can be generated at the shock–streamer interaction region (e.g., Chao et al. 2008); a streamer density model (Newkirk 1961), however, gives type II heights much larger than those indicated by the coronal structure deflection as shown in Figure 1 and an unrealistic shock speed $\sim$1500 km s^{-1}.) Four curves corresponding to the emissions upstream and downstream of the shock at the fundamental and harmonic plasma frequencies are obtained from the linear fit of the type II distances, as shown in Figure 4: we simply divide the frequency–time curve by a factor of 2 to get the curve at the fundamental plasma frequency upstream of the shock, and then a factor of 1.26 (the observed frequency ratio of the splitting bands) times each of these two curves gives their counterparts downstream of the shock. These curves successfully establish the connectivity between the metric and DH type II emissions from both the upstream and downstream regions of the shock, although the curves are obtained only from the harmonic band upstream of the shock. It is generally accepted that DH and lower frequency type II bursts are produced by CME-driven shocks (e.g., Cane et al. 1987; Gopalswamy et al. 2000). A causal relationship between metric and DH type II bursts would imply that the associated metric type II burst is CME driven as well.

The shock speed in combination with the shock Mach number gives $v_A = 419$ km s^{-1} if the shock is perpendicular and $v_A = 489$ km s^{-1} if the shock is parallel. The starting frequency of the type II burst corresponds to a heliocentric distance of 1.49 $R_\odot$. At this distance, the CME speed is about 600 km s^{-1} (see Figure 3), sufficiently larger than the Alfvén speed. The timescale t_s within which a piston-driven pressure wave steepens into a shock can be expressed as (Vršnak & Cliver 2008)

$$t_s = \frac{(2M_A + 2)t_a}{3M_A},$$

where t_a is the acceleration timescale of the piston. The shock formation time is comparable to the acceleration time ($t_s \sim t_a$) when $M_A \sim 1$, so a shock will form almost immediately once the piston achieves the Alfvén speed. Therefore, a shock must have been created by the fast motion of the CME, which is confirmed by the distant deflection of coronal structures (see Figure 1). The deflection occurs only about 2.6 minutes before the metric type II onset and continues during the type II burst. The good timing between the distant coronal structure deflection and the metric type II burst shows that the metric type II burst originates from the CME-driven shock. Further confidence is provided by the agreement between the shock propagation determined from the type II burst and the shock height–time profile obtained from the remote streamer deflection (see Figure 3, right).

3. CONCLUSION

We have investigated the relationship between the shock driven by the 2007 December 31 CME and the associated metric type II burst, based on unprecedented high-cadence observations of *STEREO*/SECCHI. The results demonstrate unambiguously that the metric type II burst is caused by the CME-driven shock; the shock is formed in the low corona and propagates far into interplanetary space.

The research was supported by the *STEREO* project under grant NAS5-03131. We acknowledge the use of *GOES* and Learmonth data and thank W. C. Erickson, S. M. White, and T. S. Bastian for providing the BIRS data.

REFERENCES

Bougeret, J.-L., et al. 1998, Geophys. Res. Lett., 25, 2513
Bougeret, J.-L., et al. 2008, Space Sci. Rev., 136, 487
Cane, H. V., McGuire, R. E., & von Rosenvinge, T. T. 1986, ApJ, 301, 448
Cane, H. V., Sheeley, N. R. Jr., & Howard, R. A. 1987, J. Geophys. Res., 92, 9869
Cane, H. V., et al. 1981, Geophys. Res. Lett., 8, 1285
Chao, K.-S., et al. 2008, A&A, 491, 873
Cliver, E. W. 1999, J. Geophys. Res., 104, 4743
Cliver, E. W., Nitta, N. V., Thompson, B. J., & Zhang, J. 2005, Solar Phys., 225, 105
Cliver, E. W., Webb, D. F., & Howard, R. A. 1999, Solar Phys., 187, 89
Cohen, C. M. S., et al. 1999, Geophys. Res. Lett., 26, 2697
Erickson, W. C. 1997, PASA, 14, 278
Gopalswamy, N., et al. 1998, J. Geophys. Res., 103, 307
Gopalswamy, N., et al. 2000, Geophys. Res. Lett., 27, 1427
Gosling, J. T., et al. 1974, J. Geophys. Res., 79, 4581
Howard, R. A., et al. 2008, Space Sci. Rev., 136, 67
Klein, K.-L., Khan, J. I., Vilmer, N., Delouis, J.-M., & Aurass, H. 1999, A&A, 346, L53
Kundu, M. R. 1965, Solar Radio Astronomy, (New York: Interscience), 362
Liu, Y., et al. 2008, ApJ, 689, 563
Mason, G. M., Mazur, J. E., & Dwyer, J. R. 1999, ApJ, 525, L133
Nelson, G. J., & Melrose, D. B. 1985, in Solar Radiophysics: Studies of Emission from the Sun at Metre Wavelengths, ed. D. J. McLean & N. R. Labrum (Cambridge: Cambridge Univ. Press), 333
Newkirk, G., Jr. 1961, ApJ, 133, 983
Payne-Scott, R., Yabsley, D. E., & Bolton, J. G. 1947, Nature, 160, 256
Pick, M., et al. 2006, Space Sci. Rev., 123, 341
Priest, E. R. 1982, Solar Magnetohydrodynamics, (Dordrecht: Reidel)
Reames, D. V. 1999, Space Sci. Rev., 90, 413
Saito, K., Poland, A. I., & Munro, R. H. 1977, Solar Phys., 55, 121
Sheeley, N. R., Jr., Hakala, W. N., & Wang, Y.-M. 2000, J. Geophys. Res., 105, 5081
Smerd, S. F., Sheridan, K. V., & Stewart, R. T. 1975, Astrophys. Lett., 16, 23
Vourlidas, A., Wu, S. T., Wang, A. H., Subramanian, P., & Howard, R. A. 2003, ApJ, 598, 1392
Vršnak, B., Aurass, H., Magdalenić, J., & Gopalswamy, N. 2001, A&A, 377, 321
Vršnak, B., & Cliver, E. W. 2008, Solar Phys., 253, 215
Vršnak, B., Magdalenić, J., Aurass, H., & Mann, G. 2002, A&A, 396, 673
Vršnak, B., Ruždjak, V., Zlobec, P., & Aurass, H. 1995, Solar Phys., 158, 331
Wild, J. P., Murray, J. D., & Rowe, W. C. 1953, Nature, 172, 533
Zhang, J., Dere, K. P., Howard, R. A., Kundu, M. R., & White, S. M. 2001, ApJ, 559, 452